

See discussions, stats, and author profiles for this publication at: <https://www.researchgate.net/publication/7453109>

# Multicomponent Cationic Lipid–DNA Complex Formation: Role of Lipid Mixing

ARTICLE *in* LANGMUIR · JANUARY 2006

Impact Factor: 4.46 · DOI: 10.1021/la052077c · Source: PubMed

CITATIONS

51

READS

24

## 4 AUTHORS:



**Giulio Caracciolo**

Sapienza University of Rome

**115** PUBLICATIONS **1,616** CITATIONS

SEE PROFILE



**Daniela Pozzi**

Sapienza University of Rome

**121** PUBLICATIONS **1,589** CITATIONS

SEE PROFILE



**Heinz Amenitsch**

Graz University of Technology

**375** PUBLICATIONS **8,372** CITATIONS

SEE PROFILE



**Ruggero Caminiti**

Sapienza University of Rome

**250** PUBLICATIONS **4,969** CITATIONS

SEE PROFILE

# Multicomponent Cationic Lipid–DNA Complex Formation: Role of Lipid Mixing

Giulio Caracciolo,<sup>\*,†</sup> Daniela Pozzi,<sup>†</sup> Heinz Amenitsch,<sup>‡</sup> and Ruggero Caminiti<sup>†</sup>

*Dipartimento di Chimica, Università degli Studi di Roma “La Sapienza”, Rome, Italy 00185, and Institute of Biophysics and X-ray Structure Research, Austrian Academy of Sciences, Graz, Austria*

*Received July 29, 2005. In Final Form: October 12, 2005*

Multicomponent cationic lipid–DNA complexes (lipoplexes) were prepared by adding linear DNA to mixed lipid dispersions containing two populations of binary cationic liposomes and characterized by means of small angle X-ray scattering (SAXS). Four kinds of cationic liposomes were used. The first binary lipid mixture was made of the cationic lipid (3′[N-(N′,N′-dimethylaminoethane)-carbamoyl]cholesterol (DC–Chol) and the neutral helper lipid dioleoylphosphocholine (DOPC) (DC–Chol/DOPC liposomes), the second one of the cationic 1,2-dioleoyl-3-trimethylammonium-propane (DOTAP) and the neutral dioleoylphosphatidylethanolamine (DOPE) (DOTAP/DOPE liposomes), the third one of DC–Chol and DOPE (DC–Chol/DOPE liposomes), and the fourth one of DOTAP and DOPC (DOTAP/DOPC liposomes). Upon DNA-induced fusion of liposomes, large lipid mixing at the molecular level occurs. As a result, highly organized mixed lipoplexes spontaneously form with membrane properties intermediate between those of starting liposomes. By varying the composition of lipid dispersions, different DNA packing density regimes can also be achieved. Furthermore, occurring lipid mixing was found to induce hexagonal to lamellar phase transition in DOTAP/DOPE membranes. Molecular mechanisms underlying experimental findings are discussed.

## 1. Introduction

Cationic lipid–DNA complexes, named lipoplexes in the scientific community, are extensively used for cell transfection in vitro and are also promising candidates for in vivo gene therapy.<sup>1–3</sup>

Lipoplexes mimic natural viruses in their ability to act as carriers of DNA, the main advantages being ease of production and potential for transfecting large pieces of DNA into cells.<sup>1–3</sup>

Lipoplexes form spontaneously when adding DNA to dispersions of binary cationic liposomes (CLs, closed lipid bilayer shells of cationic and neutral “helper” lipids).<sup>4</sup>

By using a plethora of experimental techniques, a variety of structures were observed with topology controlled by the choice of the helper lipid.<sup>5</sup> In the multilamellar L<sub>α</sub><sup>C</sup> phase, DNA chains are condensed between opposing cationic lipid membranes in the liquid-crystalline L<sub>α</sub> phase, whereas the inverted hexagonal H<sub>II</sub><sup>C</sup> phase is comprised of lipid-coated DNA strands arranged on a hexagonal lattice.<sup>5–7</sup>

Despite the relevant contribution clarifying the structure and morphology of lipoplexes,<sup>4–7</sup> little is known about the mechanisms of formation. This lack of knowledge is essentially due to the high complexity of the self-assembly

process.<sup>8–10</sup> Nevertheless, it is well accepted that decoding the underlying molecular mechanisms may yield new therapeutic means for a large quantity of disorder.<sup>11</sup>

In this paper, we looked at the simultaneous interaction of two populations of CLs with linear DNA. CL–DNA complexes were characterized by means of high-resolution synchrotron small angle scattering (SAXS). Here we show that, upon lipoplex formation, a large lipid mixing occurs. Lipid mixing occurring during DNA-induced fusion of single species dipalmitoylphosphatidylcholine (DPPC) vesicles has been recently reported.<sup>12</sup> Nevertheless, as far as we know, no evidence of lipid mixing upon DNA-induced fusion of very different liposomal formulations has been provided so far. Here we also identified lipid mixing as the driving force for phase transitions in nonlamellar lipid systems.

Upon complexation, multicomponent lipoplexes emerge with highly specific physical properties. It was an attractive result. Indeed, the engineering of multicomponent lipoplexes, incorporating the specific properties of very different lipid species, may represent the starting point to rationally design highly specific gene vectors.<sup>13–15</sup>

To this end, we chose cationic liposomes exhibiting different lipid headgroups and a number of systematic

\* To whom correspondence should be addressed. E-mail: g.caracciolo@caspur.it.

<sup>†</sup> Università degli Studi di Roma “La Sapienza”.

<sup>‡</sup> Austrian Academy of Sciences.

(1) Felgner, P. L.; Gadek, T. R.; Holm, M.; Roman, R.; Chan, H. W.; Wenz, M.; Northrop, J. P.; Ringold, G. M.; Danielsen, M. *Proc. Natl. Acad. Sci. U.S.A.* **1987**, *84*, 7413.

(2) Felgner, P. L. *Sci. Am.* **1997**, *276*, 102.

(3) Lasic, D. *Liposomes in Gene Delivery*; CRC Press: Boca Raton, FL, 1997.

(4) Salditt, T.; Koltover, I.; Rädler, J. O.; Safinya, C. R. *Phys. Rev. Lett.* **1997**, *79*, 2582.

(5) Koltover, I.; Salditt, T.; Rädler, J. O.; Safinya, C. R. *Science* **1998**, *281*, 78.

(6) Koltover, I.; Salditt, T.; Safinya, C. R. *Biophys. J.* **1999**, *77*, 915.

(7) Artzner, F.; Zantl, R.; Rapp, G.; Rädler, J. O. *Phys. Rev. Lett.* **1998**, *81*, 5015.

(8) Huebner, S.; Battersby, B. J.; Grimm, R.; Cevc, G. *Biophys. J.* **1999**, *76*, 3158.

(9) Barreleiro, P. C. A.; May, R. P.; Lindman, B. *Faraday Discuss.* **2002**, *122*, 191.

(10) Barreleiro, P. C. A.; Lindman, B. *J. Phys. Chem. B* **2003**, *107*, 6208.

(11) Kinnunen, P. K. J.; Holopainen, J. M. *Bioscience Rep.* **2000**, *6*, 465.

(12) Hayes, M. E.; Gorelov, A. V.; Dawson, K. A. *Prog. Colloid Polym. Sci.* **2001**, *118*, 243.

(13) Rubanyi, G. M. *Mol. Asp. Med.* **2001**, *22*, 113.

(14) Prata, C. A. H.; Zhau, Y.; Barthelemy, P.; Li, Y.; Luo, D.; McIntosh, T. J.; Lee, S. J.; Grinstaff, M. W. *J. Am. Chem. Soc.* **2004**, *126*, 12196.

(15) McManus, J.; Rädler, J. O.; Dawson, K. A. *J. Am. Chem. Soc.* **2004**, *126*, 15966.

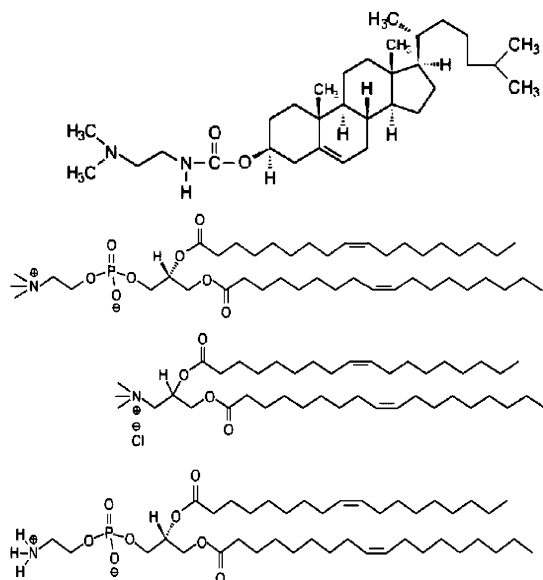


**Figure 1.** Chemical structure of the lipids used: DC-Chol, DOPC, DOTAP, and DOPE (from the top to the bottom).

differences in physical–chemical parameters.<sup>16</sup> We have used cationic lipids (3-[N-(N,N-dimethylaminoethane)-carbamoyl]cholesterol (DC-Chol) and 1,2-dioleoyl-3-trimethylammonium-propane (DOTAP) and neutral helper lipids dioleoylphosphocholine (DOPC) and dioleoylphosphatidylethanolamine (DOPE).

The chemical structure of the lipids used is displayed in Figure 1.

## 2. Materials and Methods

**I. Sample Preparation.** Multilamellar DC-Chol/DOPC (A), DOTAP/DOPE (B), DC-Chol/DOPE (C), and DOTAP/DOPC (D) CLs were routinely prepared.<sup>17</sup> Briefly, each binary mixture, at a molar ratio of neutral lipid in the bilayer  $\Phi = (\text{neutral lipid}/\text{total lipid}) (\text{mol/mol}) = 0.5$ , was dissolved in chloroform and the solvent was evaporated under a stream of nitrogen and then under a vacuum for 12 h. The obtained lipid films were hydrated with the appropriate amount of Tris-HCl buffer solution ( $10^{-2}$  M, pH 7.4) to achieve the desired final concentration of 100 mg/mL. The solutions were incubated at 30 °C for 6 h to allow formation of CLs. Calf thymus Na-DNA solution (10 mg/mL) was sonicated inducing a DNA fragmentation with length distribution between 500 and 1000 bp which was determined by gel electrophoresis. All of the lipids were purchased from Avanti Polar Lipids (Alabaster, AL), whereas the DNA was purchased from Sigma (St. Louis, MO). Then, we mixed initially separated A and B vesicles at seven relative molar ratios  $R_{AB} = A/(A+B) = 0, 0.2, 0.4, 0.5, 0.6, 0.8$ , and 1. The first and the latter  $R_{AB}$  values refer to pure B and A vesicles, respectively. Mixed lipid dispersions were equilibrated at 30 °C for 36 h. The same procedure was applied to prepare mixed C–D and B–C dispersions at the molar ratios  $R_{CD} = C/(C+D) = 0, 0.2, 0.4, 0.5, 0.6, 0.8$ , and 1 and  $R_{BC} = C/(B+C) = 0, 0.2, 0.4, 0.5, 0.6, 0.8$ , and 1. By mixing adequate amounts of the DNA solution to suitable volumes of A–B and C–D mixed dispersions, self-assembled lipoplexes at charge ratio  $\rho = (\text{lipid charge}/\text{DNA charge}) = 0.5$  were obtained. B–C-DNA lipoplexes were prepared at three charge ratios  $\rho = 0.5, 1$ , and 2. After mixing with the DNA, all lipoplexes were incubated at 30 °C for 36 h.

**II. SAXS Measurements.** All SAXS measurements were performed at the Austrian SAXS station of the synchrotron light source ELETTRA (Trieste, Italy).<sup>18</sup> SAXS patterns were recorded with a gas detector based on the delay line principle covering a  $q$  range ( $q = 4\pi \sin(\theta)/\lambda$ ) of between 0.05 and  $1.5 \text{ \AA}^{-1}$ . The angular calibration of the detector was performed with silver-behenate [ $\text{CH}_3(\text{CH}_2)_{20}\text{-COOAg}$ ] whose  $d$  corresponds to  $58.38 \text{ \AA}$ . The

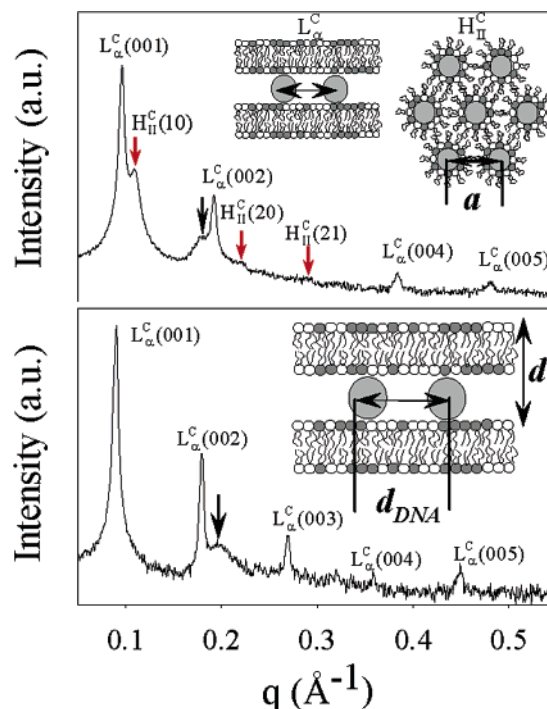


**Figure 2.** Bottom panel: SAXS pattern of DC-Chol/DOPC-DNA lipoplex (A-DNA in the text,  $R_{AB} = 1$ ). In the inset, schematics of the  $L_\alpha^C$  lamellar phase is depicted. Top panel: SAXS pattern of DOTAP/DOPE-DNA lipoplex (B-DNA in the text,  $R_{AB} = 0$ ) arising from coexisting  $L_\alpha^C$  and the  $H_\Pi^C$  phases. Red arrows indicate the Bragg reflections of the  $H_\Pi^C$  phase. In the inset schematics of both the phases is displayed. DNA peak of the lamellar phase is marked by a black arrow in both the panels.

unoriented samples were sealed in 1.5 mm diameter glass X-ray capillaries. All SAXS measurements were performed at 26 °C, and temperature was controlled close to the capillary by a KPR-Peltier module (Anton Paar, Graz, Austria) to a precision of 0.1 °C. Exposure times were between 100 and 500 s. No evidence of radiation damage was observed in any sample at these exposure times. The Tris-HCl bulk solution was subtracted as background from the collected data.

## 3. Results and Discussion

SAXS pattern of A-DNA lipoplexes ( $\rho = 0.5$ ,  $R_{AB} = 1$ ) is shown in Figure 2 (bottom panel). The sharp periodically spaced peaks at  $q_{00n}$  are caused by alternating lipid bilayer-DNA monolayer structure with periodicity  $d = 2\pi/q_{001} = 69.9 \text{ \AA}$ . DNA monolayers are ordered in a one-dimensional lattice with a well-defined spacing  $d_{DNA}$  between the DNA chains. Nevertheless, the DNA peak (arrow in Figure 2, bottom panel) is much broader than the lamellar ones because the DNA rods form a two-dimensional smectic liquid crystal which is less stable against thermal disorder than the three-dimensional smectic of the bilayer-DNA structure.<sup>19</sup> The calculated DNA spacing was  $d_{DNA} = 30.5 \text{ \AA}$ .

SAXS pattern of B-DNA lipoplexes ( $\rho = 0.5$ ,  $R_{AB} = 0$ ) is shown in Figure 2 (top panel). Lamellar peaks at  $q_{00n}$  arising from the lamellar  $L_\alpha^C$  phase ( $d = 2\pi/q_{001} = 65.2 \text{ \AA}$ ) were detected. Systematic absence of the third-order Bragg peak in the SAXS pattern can be observed.

(17) Caracciolo, G.; Sadun, R.; Caminiti, R.; Pisani, M.; Bruni, P.; Francescangeli, O. *Chem. Phys. Lett.* **2004**, *397*, 138.

(18) Amenitsch, H.; Bernstorff, S.; Kriechbaum, M.; Lombardo, D.; Mio, H.; Rappolt, M.; Lagner, P. *J. Appl. Crystallogr.* **1997**, *30*, 872.

(19) Salditt, T.; Koltov, I.; Rädler, J. O.; Safinya, C. R. *Phys. Rev. E* **1998**, *58*, 889.

**Table 1. Lamellar  $d$ -spacing and DNA-DNA Distance,  $d_{\text{DNA}}$ , of A–B–DNA Mixed Lipoplexes as a Function of  $R_{\text{AB}}$** 

$R_{\text{AB}}$	$d(\text{\AA})$	$d_{\text{DNA}}(\text{\AA})$
0	65.2	34.3
0.2	66.1	n.d. <sup>a</sup>
0.4	66.8	40.6
0.5	67.4	35.7
0.6	67.8	30.8
0.8	69.0	30.5
1	69.9	30.5

<sup>a</sup> Not detectable

The DNA peak (black arrow in Figure 2, top panel) occurring at  $q_{\text{DNA}} = 0.183 \text{ \AA}^{-1}$  ( $d_{\text{DNA}} = 34.3 \text{ \AA}$ ) was also evident. In addition, we observed Bragg peaks of a 2D hexagonal phase positioned at  $q_{10} = 0.109 \text{ \AA}^{-1}$ ,  $q_{20} = 0.218 \text{ \AA}^{-1}$ ,  $q_{21} = 0.287 \text{ \AA}^{-1}$  (marked by red arrows in Figure 2, top panel).

We calculated a unit cell spacing of  $a = 4\pi/[(3)^{0.5}q_{10}] = 66.6 \text{ \AA}$ . The  $q_{11}$  reflection, expected at  $q = \sqrt{3} q_{10} = 0.188 \text{ \AA}^{-1}$ , is superimposed to the second-order Bragg peak of the lamellar phase and could not be detected. Our findings are in excellent agreement with the results previously reported by Koltover et al.,<sup>5</sup> who found coexistence, at  $\Phi = 0.65$ , of  $L_{\alpha}^{\text{C}}$  and  $H_{\text{II}}^{\text{C}}$  phases. Thus, our data show that phase coexistence begins at  $0.41 < \Phi < 0.5$ . Unambiguous support to the phase coexistence of  $L_{\alpha}^{\text{C}}$  and  $H_{\text{II}}^{\text{C}}$  phases was also provided by the DNA packing density within A–B–DNA lipoplexes as resulting from the SAXS pattern in Figure 3. As well established,<sup>6</sup> the surface charge density,  $\sigma_{\text{M}}$ , is the physical constraint regulating the DNA in plane rod lattice. More in detail,  $d_{\text{DNA}}$  diminishes monotonically as a function of increasing  $\sigma_{\text{M}}$ . Moving from  $R_{\text{AB}} = 0$  (pure B-DNA lipoplexes) to  $R_{\text{AB}} = 1$  (pure A-DNA lipoplexes), one would therefore expect a monotonic change in  $d_{\text{DNA}}$  due to the continuous change in surface charge density of the emerging multicomponent lipid membrane. Conversely,  $d_{\text{DNA}}$  first increases, passes through a maximum at  $R_{\text{AB}} = 0.4$ , and then falls off until a plateau is reached (Table 1). Why should  $\sigma_{\text{M}}$  exhibit such an unexpected jump? This apparently anomalous behavior really depends on the phase coexistence of  $L_{\alpha}^{\text{C}}$  and  $H_{\text{II}}^{\text{C}}$  phases. For  $0 < R_{\text{AB}} < 0.4$ ,  $d_{\text{DNA}}$  moves from 34.3 to 40.6  $\text{\AA}$ , whereas for  $0.4 < R_{\text{AB}} < 1$ , it decreases monotonically moving from 40.6 to 30.5  $\text{\AA}$ . It means that, for  $0 < R_{\text{AB}} < 0.4$ , the effective molar fraction of lipid molecules assembled in the lamellar phase is lower than unity resulting in a DNA packing density higher than that one would expect in all lamellar complexes at the same charge ratio. Thus, due to the phase coexistence of Figure 2 (top panel), the effective charge ratio is lower than  $\rho = 0.5$  and shorter  $d_{\text{DNA}}$  spacings are observed.

SAXS measurements on mixed A–B dispersions with no DNA added revealed (data not reported) that, upon mixing of A and B, no fusion occurs. It means that electrostatic charges localized on the surface of liposome create a repulsive barrier which dominates over short-range attractive van der Waals forces and prevents membranes aggregation and fusion.<sup>12,20</sup>

Adding DNA to mixed A–B dispersions produces major changes in the lipid structure.

SAXS patterns of Figure 3 ( $0.4 < R_{\text{AB}} < 0.8$ ) show that, for each  $R_{\text{AB}}$  value, only mixed A–B lipoplexes ( $\rho = 0.5$ ) exist. In principle, the presence of A-DNA and B-DNA rich domains cannot be excluded at all. Nevertheless,

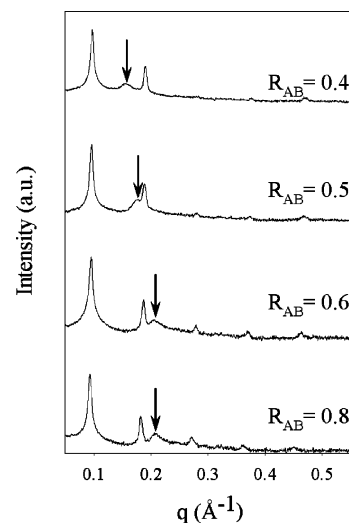


**Figure 3.** SAXS patterns of mixed A–B–DNA lipoplexes (A: DC–Chol/DOPC; B: DOTAP/DOPE) as a function of the relative molar fraction  $R_{\text{AB}} = A/(A + B)$ . As  $R_{\text{AB}}$  increases, DNA peak (marked by arrows) moves to higher  $q$  values, i.e., shorter DNA spacings, as a result of higher surface charge density of the lipid membrane.<sup>6</sup>

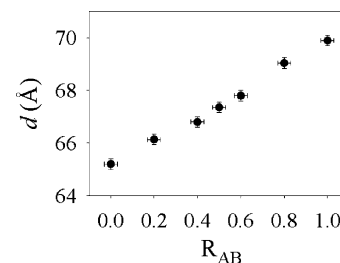


**Figure 4.** Lamellar periodicity  $d$  of A–B–DNA lipoplexes (A: DC–Chol/DOPC; B: DOTAP/DOPE) as a function of  $R_{\text{AB}}$ .

several reasons arise that a complete lipid mixing at the molecular level occurs. First of all, the SAXS patterns of Figure 3 do not arise from the superposition of the patterns of A-DNA and B-DNA lipoplexes of Figure 2. In addition, the lamellar spacing  $d$  varies monotonically as a function of  $R_{\text{AB}}$  (Figure 4), whereas the full width at half-maximum (fwhm) of all the Bragg peaks is roughly the same (not reported). Further support to this interpretation is provided by DNA packing density within mixed lipoplexes. As established,<sup>21,22</sup> lamellar lipoplexes adjust the interaxial spacing  $d_{\text{DNA}}$  in order to minimize the total free energy by separating the DNA strands. If lipid mixing was not almost complete and different DNA packing density regimes existed, there distinct DNA peaks would be certainly detected.<sup>21,22</sup> In contrast, we noted that all of the SAXS patterns of Figure 3 exhibit a single DNA peak (marked by arrow).

All these observations allowed us to conclude that, upon liposomes fusion, there is a large onset of membrane mixing and that the emerging lipid system has physical membrane properties intermediate between those of A and B.

Undoubtedly, A–B–DNA lipoplexes can exist only if A and B break up during complex formation.<sup>19</sup> As liposomes fusion was not observed merely by mixing A and B, it is therefore the DNA which allows the liposomes to come into contact, aggregate and fuse by reducing the inter-

(20) Kennedy, M. T.; Pozharski, E. V.; Rakhmanova, V. A.; MacDonald, R. C. *Biophys. J.* **2000**, 78, 1620.

(21) Safinya, C. R. *Curr. Opin. Struct. Biol.* **2001**, 11, 440.  
(22) Caracciolo, G.; Pozzi, D.; Caminiti, R.; Congiu Castellano, A. *Eur. Phys. J. E* **2003**, 10, 331.



membrane repulsive barrier due to electrostatic, steric and hydration forces.<sup>12</sup>

Recently Hayes et al.<sup>12</sup> reported on the DNA-induced fusion of DPPC vesicles in the presence of calcium cations and showed that it is the calcium-mediated interaction of liposomes with DNA that promotes lipid mixing.

In the case of CLs, the counterion release mechanism is the driving force for lipoplex formation.<sup>6</sup> During complexation, both the lipids and the DNA release their counterions into the bulk solution with remarkable entropic gain (about  $1 K_B T$  per released counterion). Although molecular mechanisms underlying CL-DNA and DPPC- $\text{Ca}^{2+}$ -DNA complexes formation are deeply different, here we emphasize that, it is the DNA-induced liposomes fusion the essential prerequisite which leads to lipid mixing.

As far as we know, the data presented have provided the first experimental evidence of lipid mixing occurring upon DNA-induced fusion of very different liposomal formulations. Such a mixing, like any self-assembling process, is driven by thermodynamics and requires a decrease of free energy to be spontaneous. Large multilamellar cationic vesicles in aqueous media, as those used in the present study, are considered as thermodynamically stable and, due to their net charge, very likely represent equilibrium structures.<sup>23</sup> Previous studies have investigated the kinetics of lipoplexes formation.<sup>9,10</sup> Although a detailed picture of the molecular mechanisms underlying formation is still lacking, the existence of a multistep mechanism is well accepted.<sup>10,20,24</sup> In the first step, the negatively charged phosphate groups of DNA interact with the cationic lipid headgroups by electrostatic interactions. This process is very fast and occurs within milliseconds.<sup>10</sup> DNA adsorbing to one side of the lipid bilayer probably induces an asymmetry in packing pressure between the outer and inner leaflets of the lipid bilayer.<sup>8</sup> This stress is likely to result from dehydration of lipid headgroups<sup>11</sup> or, alternatively, from the reduction of the cationic lipid headgroup area when positive charge is neutralized by the negative charged DNA molecules on only one side of the bilayer.<sup>8</sup> It has been hypothesized that this asymmetry should tend to destabilize the membrane inducing local adhesion and fusion of liposomes which allows for lipid mixing.<sup>8-12,24</sup> On a longer time scale (seconds) the DNA-lipid complex continues to grow leading to multilamellar aggregates.<sup>8,9</sup> This scenario is readily compatible with our structural results. Indeed, when adding linear DNA to mixed lipid dispersions containing two distinct populations of binary cationic liposomes, only mixed A-B-DNA lipoplexes were found to exist which unequivocally indicated contact and fusion of A and B membranes. The present results have provided additional information in that high mixing of lipids between A and B liposomes occurred. Indeed no A-DNA and B-DNA lipoplexes were observed within the sample volume and the four-component lipid bilayer exhibited physical properties, namely surface charge density and bilayer thickness (Figure 4), intermediate between those of A and B membranes, and as a matter of fact, mixing of similar lipids in aggregates is the rule for thermodynamically stable phases. Thus, we have provided evidence that, upon fusion of A and B liposomes, the lipid bilayer, being a fluid mixture, allowed for lateral diffusion of lipid molecules leading to a spatial distribution of the four lipid species, on average, uniform.

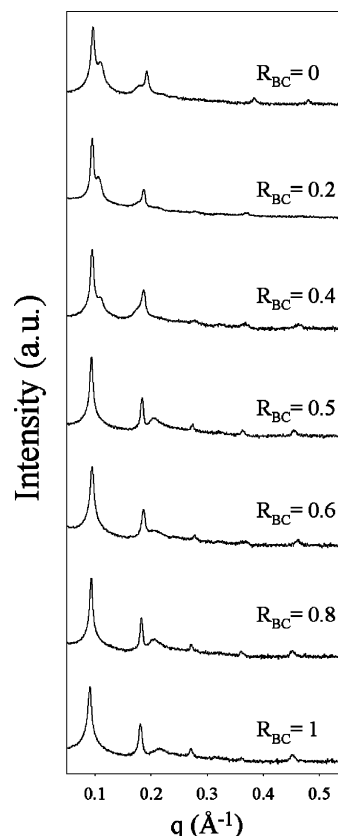


**Figure 5.** SAXS patterns of ternary B-C-DNA lipoplexes (B: DOTAP/DOPE; C: DC-Chol/DOPE) as a function of the relative molar fraction  $R_{BC} = C/(B + C)$ . As  $R_{BC}$  increases, the percentage of  $H_{II}^C$  phase in mixed lipoplexes decreases. At  $R_{BC} = 0.5$  only lamellar lipoplexes exist.

Significantly, we observed that the inner structure of B-DNA lipoplexes (coexisting  $L_\alpha^C$  and  $H_{II}^C$  phases) closely resemble that of pure B membranes (coexisting  $L_\alpha$  and  $H_{II}$  phases) with the water space inside the inverse micelle of the  $H_{II}$  phase and the interbilayer water region of the  $L_\alpha$  phase both filled by DNA (schematics in Figure 2, top panel). It means that, upon complexation, DNA lets B liposomes break up and penetrates the accessible water regions.

Conversely, we observed that A-B-DNA lipoplexes are only assembled in the lamellar phase. Thus, some molecular events occurring during A-B-DNA lipoplexes formation were able to induce the  $H_{II} \rightarrow L_\alpha$  phase transition of B membranes first assembled in the  $H_{II}$  phase. Although DNA-induced liposomes fusion is the first step in the lipoplex formation, it cannot be the DNA that induces the observed hexagonal to lamellar phase transition.

By comparing the different phase behavior of B and A-B lipid dispersions upon lipoplex formation, we argue that lipid mixing is the driving force which induces the observed phase transition. In fact, lipid mixing occurring upon DNA-induced fusion of B vesicles could not produce any detectable structural change. At the molecular level, lipid mixing occurring during A and B liposomes fusion can produce major structural changes. Indeed, cationic DOTAP and DC-Chol as well as neutral DOPC have a cylindrical shape with the cross section area of headgroups approximately equal to the hydrophobic chain area. Thus, they tend to self-assemble into lamellar structures with a spontaneous curvature  $C_0 = 1/R_0 = 0$ .<sup>25</sup> DOPE, due to

(23) Hauser, H. *Biochim. Biophys. Acta* **1984**, 772, 37.

(24) Oberle, V.; Bakowsky, U.; Zuhorn, I. S.; Hoekstra D. *Biophys. J.* **2000**, 79, 1447.

(25) Israelachvili, J. *Intermolecular and surface forces*; Academic Press: London, 1991.

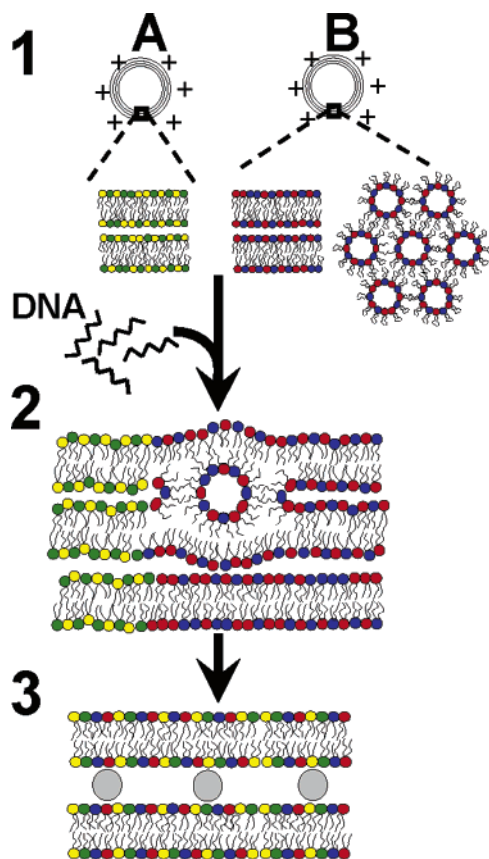


**Figure 6.** Mechanism of formation of mixed multicomponent lipoplexes. In the first step (1), DNA is added to a mixed dispersion containing noninteracting positively charged A and B liposomes. In the second step (2), DNA induces local aggregation and fusion of A and B.<sup>8–12,19,20,24</sup> In the sketch, a rod of the hexagonal phase of B (red and blue molecules) fuse with the bilayer structure of A (green and yellow molecules). Upon fusion, large lipid mixing occurs. Lipid mixing diminishes the percentage of DOPE in the emerging bilayer with respect to that of pure B membranes and promotes the hexagonal to lamellar phase transition by controlling the curvature of membranes. As a result, only mixed A–B lipoplexes exist (3). The same mechanism describes the formation of mixed B–C–DNA lipoplexes.

its cone-like molecular arrangement, gives rise to a negative natural curvature and forms inverted hexagonal phases. Furthermore, it is well established that the shape of the molecule determines the curvature of the membrane and the structure of the self-assembly. Thus, lipid mixing gradually reduces the relative molar percentage of DOPE in the emerging lipid bilayer with respect to pure B membranes and the lamellar phase becomes favored with respect to the inverted hexagonal one.<sup>5</sup> Lipid mixing therefore induces the  $H_{II} \rightarrow L_{\alpha}$  phase transition by controlling the spontaneous curvature of the emerging membranes.<sup>5</sup>

Unambiguous support to this interpretation was provided by SAXS experiments replicated on B–C ternary lipoplexes as a function of  $R_{BC}$ . As shown in Figure 5, C–DNA lipoplexes show a highly organized lamellar structure with periodicity  $d = 69 \text{ \AA}$  and DNA spacing  $d_{DNA} = 29.2 \text{ \AA}$ .

Ternary B–C–DNA lipoplexes formed coexisting  $L_{\alpha}^C$  and the  $H_{II}$  phases up to  $R_{BC} = 0.4$ . This is because, for  $R_{AB} = R_{BC}$ , B–C–DNA lipoplexes have higher molar percentage of DOPE in the bilayer than A–B–DNA lipoplexes (DOPC substituted by DOPE). As a result,  $H_{II} \rightarrow L_{\alpha}$  phase transition cannot be completed up to  $R = 0.5$ .

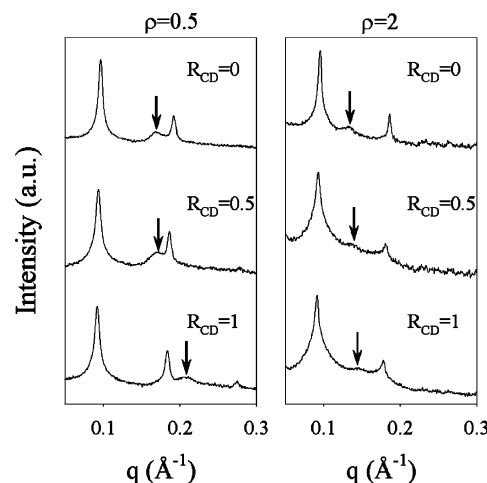


**Figure 7.** SAXS patterns of C–D–DNA lipoplexes (C: DC–Chol/DOPE; D: DOTAP/DOPC) as a function of the relative molar fraction  $R_{CD}$  at two distinct charge ratios ( $\rho = 0.5$  left panel and  $\rho = 2$  right panel). The DNA mobile peak is indicated by arrows. At the same  $R_{CD}$  value, higher charge ratio results in lower DNA packing density and the DNA peak moves to higher  $q$  values. To clarify the  $q$ -range has been restricted to  $q = 0.3 \text{ \AA}^{-1}$ .

Accordingly, we identified the structural pathway leading to phase transition that is schematically described in Figure 6.

In addition, we observed that the interaxial distance of C–DNA lipoplexes is shorter than that of both A–DNA and B–DNA lipoplexes.<sup>21</sup> Since the interaxial DNA–DNA distance is a function of  $\sigma_M$ ,<sup>21</sup> our results show that the surface charge density of DC–Chol/DOPE liposomes, is higher than that of all of the lipoplexes investigated in the present work. It could be a central point. Indeed, several recent reports have addressed the importance of  $\sigma_M$  and the Safinya's group has recently identified it as a universal determinant of transfection behavior.<sup>26–28</sup>

Last, we underline that differences in the physical properties of lipoplexes can depend on whether liposomes interact with a small or a large amount of DNA.<sup>12,20</sup> Thus, the inner structure of mixed lipoplexes could depend on their net charge.<sup>24</sup> To clarify this matter, we replicated SAXS experiments on mixed C–D–DNA lipoplexes at the isoelectric point ( $\rho = 1$ ) and in excess of negative ( $\rho = 0.5$ ) and positive charge ( $\rho = 2$ ). Although a detailed picture of the emerging structures will be the focus of a forthcoming publication, here we anticipate that large lipid mixing occurs above and beyond the isoelectric regime and does not depend on the lipid–DNA charge ratio. Figure 7 shows the comparison between the SAXS patterns of negatively ( $\rho = 0.5$ , left panel) and positively charged ( $\rho = 2$ , right panel) C–D–DNA lipoplexes. All over the compositional range ( $0 < R_{CD} < 1$ ) only C–D–DNA mixed lipoplexes exist that are organized in the lamellar liquid-crystalline  $L_{\alpha}^C$  phase at both the charge ratios. According to the phase behavior of binary lipoplexes,<sup>6</sup> the lamellar  $d$ -spacing does not change significantly as a function of  $\rho$ . Since positively charged complexes adsorb excess lipid into their inner volume, while the negatively charged ones have surplus bulk DNA, the only difference between negatively and positively charged C–D–DNA lipoplexes is the DNA

(26) Lin, A. J.; Slack, N. L.; Ahmad, A.; Koltover, I.; George, C. X.; Samuel, C. E.; Safinya, C. R. *J. Drug Target* **2000**, *8*, 13.

(27) Ewert, K. K.; Ahmad, A.; Evans, H. M.; Safinya, C. R. *Exp. Opin. Biol. Ther.* **2005**, *5*, 33.

(28) Ahmad, A.; Evans, H. M.; Ewert, K. K.; George, C. X.; Samuel, C. E.; Safinya, C. R. *J. Gene Med.* **2005**, *7*, 739.

**Table 2. Lamellar  $d$  Spacing and DNA–DNA Distance,  $d_{\text{DNA}}$ , of C–D–DNA Mixed Lipoplexes as a Function of  $R_{\text{CD}}$**

$R_{\text{CD}}$	$d$ (Å)			$d_{\text{DNA}}$ (Å)		
	$\rho = 0.5$	$\rho = 1$	$\rho = 2$	$\rho = 0.5$	$\rho = 1$	$\rho = 2$
0	65.2	65.2	65.2	37.4	42.4	47.8
0.2	66.1	66.0	66.1	37.1	40.9	47.6
0.4	66.8	66.5	66.6	36.7	39.5	47.2
0.5	67.6	67.6	67.4	36.5	37.8	46.8
0.6	67.5	67.6	67.8	33.5	36.0	45.0
0.8	68.0	68.2	68.2	30.8	33.5	43.0
1	69.0	69.0	69.0	30.3	32.2	41.8

packing density. At the same composition of the lipid membrane, i.e., at the same  $R_{\text{CD}}$  value, positively charged C–D–DNA lipoplexes exhibit lower DNA packing density than that of negatively charged ones as unambiguously shown by the DNA peak (marked by arrow in Figure 7) that moves to lower  $q$  values, i.e., to larger  $d_{\text{DNA}}$  distances. The values of  $d$  and  $d_{\text{DNA}}$  obtained from all the SAXS patterns of C–D–DNA lipoplexes ( $R_{\text{CD}} = 0.2, 0.4, 0.5, 0.6, 0.8$ , and  $1$ ;  $\rho = 0.5, 1$ , and  $2$ ) are listed in Table 2. Positively charged lipoplexes are less stable against thermal disorder as can be seen from the SAXS patterns of Figure 7. In fact,

the broadening of the lamellar peaks of lipoplexes at  $\rho = 2$  is clearly due to an increasing disorder in weakened lipid–DNA stacks.<sup>6</sup>

As a matter of fact, the formation of both negatively and positively overcharged multicomponent lipoplexes is driven by the same physical mechanism of Figure 6, at least in the investigated charge ratio range ( $0.5 < \rho < 2$ ).

#### 4. Conclusions

In conclusion, we have shown that during lipoplex formation large lipid mixing occurs. Such a lipid mixing was also found to be the driving force for the compositionally driven hexagonal to lamellar phase transition in DOTAP/DOPE membranes.

We have also highlighted the possibility of forming highly organized lamellar lipoplexes composed of four lipid components, merely by adding DNA to dispersions containing two distinct populations of binary CLs. In the next future, the engineering of multicomponent lipoplexes, incorporating the specific properties of very different lipid species, may represent the starting point to rationally design highly specific gene vectors.<sup>13–15</sup>

LA052077C